High-resolution imaging of colloidal crystals by ptychography

Ilya Besedin, National Research Nuclear University "MEPhI", Moscow, Russia

September 5, 2013

Abstract

Feasability of the reconstruction of periodic structure by ptychography has been shown. Reconstruction of a colloid crystal structure from ptychographic data has been performed with ePIE algorithm. Hexagonal structure is cleary visible.

Contents

1 Introduction

1.1 Coherent X-ray diffraction imaging

X-ray coherent diffraction imaging is a method of high-resolution structural studies. Relying on the high degree of coherent of modern x-ray radiation sources, it extends the area of applicabilty of the principles of conventional X-ray crystallography from bulk crystals to single mesoscopic or even nanoscopic specimen. The ability to collect diffraction data from single objects instead of collecting some average data over a bigger volume puts diffraction into the region of microscopy. The resolution of this microscropy technique is theoretically limited only by diffraction, however it requires to be able to overcome the phase problem of X-ray diffraction. The first milestone in the evolution of phase-retrival algorithms is the suggestion to use an iterative scheme by Gerchberg and Saxton[4]. It was shown, that the lack of phase information can be compensated by sufficient oversampling of the diffraction pattern. A further development was to introduce real-space constraints to the reconstruction in the error-reduction algorithm[2]. The common approach was to use the "finite support" as a real space constraint, which meant that the sample had to have finite dimensions and these dimensions had to be known from some other source for a successful reconstruction. The large success of the error-reduction algorithm has promoted a lot of improvements, among which the one of the most popular was the Hibrid Input-Output algorithm[3]. One of the most prominent features of CXDI is that this imaging technique is lensless. This is very convenient, because X-ray optics are difficult to manufacture and are often the limiting factors for experiments. Nevertheless, the limited size of coherent x-ray beams and the large distances, which are required for large aperture beams to enter the Fraunhofer diffraction regime limit CXDI experiments to samples with a few tens of microns in size.

1.2 Ptychography

An alternative approach to real-space constraints is introduced in ptychographic coherent x-ray diffractive imaging, or simply ptychography. The idea of combining the advantages of microscopy with the resolution of diffraction imaging by taking diffraction pictures at various lateral position of the sample with a small beam, stems from electron microscopy [6]. If the beam is inhomogenous on the scale of the sample's features, shifting beam along the sample gives different diffraction patterns, which now depend on sample (called "object"), beam (called "probe") and beam position. The lack of phase information is compensated by setting the spacing between neighboring points on the scanning mesh less than the beam size. Because of the overlap in the illumination regions of neighboring points, which means that information from the same region gets encoded in several diffraction patterns. The first algorithms suggested to reconstruct ptychography have been non-iterative[9], while with the development of computers, iterative alghorithms like the Ptychographic Iterative Engine (PIE)[1] have become more popular. It has been soon found out, that the accuracy of the reconstruction of the samples' features is limited by the accuracy of the information on the beam. It has been shown, that the

ptychographic data allows to reconstruct not only the sample, but also the beam, using the extended Ptychography Iterative Engine (ePIE) algorithm[7]. Variations of the PIE are today the most common algorithms for reconstruction of ptychography. Here we shall give a summary of the ePIE algorithm.
a) An initial guess is given for all the 2D objects and probe functions.
b) The iteration loop starts with modeling a diffraction pattern from one of the points ρ in the mesh one one of the objects. The exit x-ray wavefront is modeled by

$$\psi_j^i(\boldsymbol{r}) = O^i(\boldsymbol{r} - \boldsymbol{\rho}_j)P^i(\boldsymbol{r}) \tag{1}$$

c) A Fourier transform is applied to the exit wavefront, which gives a model of the Fraunhofer diffraction amplitude.

$$\Psi_j^i(\boldsymbol{r'}) = \int \psi_j^i(\boldsymbol{r})e^{i\boldsymbol{r}\boldsymbol{r'}}d\boldsymbol{r} \tag{2}$$

d) The phase of the modeled diffraction amplitude is applied to the experimental diffraction intensity. This gives a diffraction amplitude, which has phase information and is consistent with experimental data.

$$\Psi_j'^i(\boldsymbol{r'}) = \sqrt{I_j(\boldsymbol{r'})}\frac{\Psi_j^i(\boldsymbol{r})}{|\Psi_j^i(\boldsymbol{r})|} \tag{3}$$

e) The corrected diffraction amplitude is inverse Fourier transformed. This gives an exit wavefront estimate, which is consistent with the experimental data.

$$\psi_j'^i(\boldsymbol{r}) = \int \Psi_j'^i(\boldsymbol{r})e^{-i\boldsymbol{r}\boldsymbol{r'}}d\boldsymbol{r} \tag{4}$$

f) The object and the probe function are updated using the corrected exit wavefront.

$$P'^{i+1}(\boldsymbol{r}) = \quad P^i(\boldsymbol{r}) + \beta_1(\psi_j'^i(\boldsymbol{r}) - \psi_j^i(\boldsymbol{r}))\frac{O^{i*}(\boldsymbol{r}-\boldsymbol{\rho})}{max(|O^i(\boldsymbol{r}-\boldsymbol{\rho})|^2)} \tag{5a}$$

$$O^{i+1}(\boldsymbol{r} - \boldsymbol{\rho_j}) = \quad O^i(\boldsymbol{r} - \boldsymbol{\rho_j}) + \beta_2(\psi_j'^i(\boldsymbol{r}) - \psi_j^i(\boldsymbol{r}))\frac{P^{i*}(\boldsymbol{r})}{max(|P^i(\boldsymbol{r})|^2)} \tag{5b}$$

g) The iteration loop is repeated for other diffraction patterns. After all diffraction patterns are applied, the algorithm repeats, until it converges.
There are some differences in the implementations of the ePIE algorithm. The initial guesses for the object can be chosen to be random, uniform or close to the actual object function, if there is some a priori knowledge about it. The order, in which the diffraction patterns are applied, can be fixed or random. Beginning with a uniform object function and using a fixed order usually improves the resolution and the convergence speed of the algorithm. The update formulas (5) can be modified. On the other hand, there are some general observations: a good initial guess of the probe function is required for convergence of the algorithm. The algorithm is not very sensitive to the β_1, β_2 parameters, and they usually only affect the convergence speed.

Ptychography relies on the assumption, that the consistency of the probe over the whole object and consistency of the reconstructed object in the overlap regions can be used as a real space constraint. Whether this constraint is enough to assure uniqueness of the inversion problem solution, depends largely on the sample and the beam. [9] One requirement that applies to the diffraction pictures is that the diffraction peaks have overlap, resulting in a smeared out diffraction pattern. In this case there is interference between the overlapping diffaction peaks, which encodes the phase difference between them. Samples with periodic structure with unit cell size much smaller than the beam size are considered difficult to reconstruct, due to the small amount of interference signal. Another problem, which may occur in weakly scattering samples, is the problem of separation of the probe and the object function. If the scattering signal is weak, errors in the detection of the transmitted beam can give a much higher contribution to the probe function, than the interference signal, which encodes the phase information. This can result in a low quality reconstruction of the probe function. A possible solution to this would be to use a strongly scattering known sample to reconstruct the probe function, and then use this probe function to reconstruct the unknown sample.

1.3 Colloidal crystals

A colloid substance is a solution of microscopic (from several nanmeters to to several microns) evenly disperesed particles in a solvent. Due to the small size of colloidal crystals, thermal (brownian) motion is quite strong. The interaction of solid colloid particles can usually be approximated by a potential, which is infinite in case two particles have an intersection, and zero otherwise. Being interacting particles with thermal motion, colloid particles can model atomic or molecular systems, and exhibit similar behaviour in structure formation: they can form liquid, cystalline and even glassy phases. This property can also be used for cheap manufacturing of nanostructures, for example, photonic crystals.

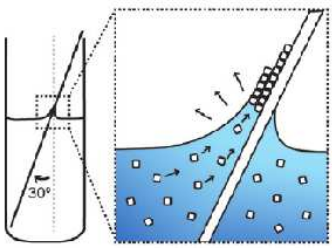

Figure 1: Illustration of the vertical deposition method. A substrate is inserted into the colloid solution. Capillary forces deform the solution surface, creating a small area, where the substrate is covered by a thin layer of the colloid solution. As the solvent evaporates, the colloid particles are deposed on the substrate surface, forming a crystalline structure.

The ability of colloid particles to self-assemble is crucial to the manufacturing process of

nanosystems. One of the approaches of creating crystalline structures is vertical deposition 1. Variation of the growth condition allows to control the crystalline properties of the samples. For many practical applications, control over the formation of defects is critical.

One of the parameters, that determine the colloid structure, is the form of the particles. The most abundant colloid particles are spherical, although other forms are also availible. Spherical particles usually form close packed structures, while cubic particles can also form cubic structures [8]. For spherical particles the free energy difference between FCC and HCP structures is very low, and in real samples both structures can be found. Common defects of crystals of spherical colloids are stacking faults [5].

2 Experiment

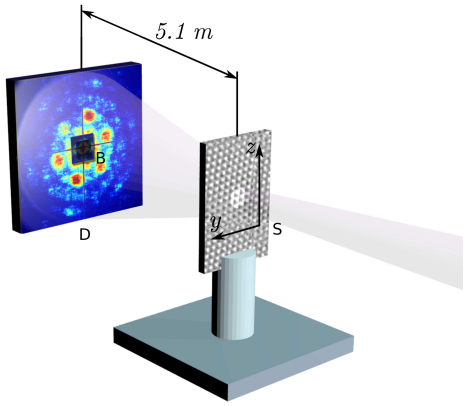

Figure 2: Setup of the ptychography experiment. The beam is focus by a pair of Kirkpatrick-Baez mirrors on the sample (S). The exit surface wave diffracted and its intensity is measured by the detector (D). Two 200 μm thick cystalline silicon beam stops (B) are installed on the center of the detector to increase the dynamic range and protect the detector from the direct beam. The sample stage has been scanned on a square mesh with 100nm step size along the y and z axes for each of the samples.

Two colloidal crystals of silica spheres have been investigated. The sphere diameters were 492 nm and 180 nm. The ptychographical imaging experiment was performed at the P10 coherence beamline of the PETRA III synchrotron source at 7.9 keV photon energy. The experimental geometry is shown on Fig. 2. The beam is focused onto the sample with a pair of KB mirrors. Intensity of the scattered beam was measured 5.1 m downstream from the samples with a MAXIPIX detector with 55 μm pixel size and 516×516 pixels resolution. The sample holder was slightly rotated around a z axis, resulting in a 2 degree angle between sample holder normal and x-ray beam.

The 492 nm sample was scanned on a 91×91 point mesh. The exposure time per frame was 0.1 s, one frame was taken in each position. The 180 nm sample was scanned on

a b

Figure 3: (a) Photo of the colloidal crystal film on the sample holder. (b) SEM image of a colloidal crystal film.

a b

Figure 4: Typical diffraction patterns of (a) 492 nm sphere colloidal crystal (b) 180 nm sphere colloidal crystal.

a 41×41 point mesh. The exposure time per frame was 0.5 s, three frames were taken in each position. The average total number of photons registered per second on the detector was $\sim 1.0 \times 10^6$ for both samples. Line scans of the intensity profiles of the focused x-ray beam in vertical and horizontal directions have been performed. The full width half maximum (FWHM) values of these profiles are 640 nm (h) and 415 nm (v). The overlap parameter is therefore in the order of 70%.

3 Results and discussion

Before the reconstruction could be started, some manupulations had to be done with the data from the detectors. Altough the MAXIPIX detector is photon-counting, the quantum efficiency of different pixels is different, and there was also quite a big number of bad pixels, so all of the frames had to be divided by a flat field image. The next step was to account for the beam stops in the center of the diffraction patterns. This was done by calculating the attenuation coefficient of a 200μm thick silicon wafer for 7.9 keV photons, and dividing the the regoins under the beam stops by this value. The calculations were carried out using the NIST X-ray mass attenuation coefficient database. The accuracy of the results of this simple procedure are questionable, due to the discontinuty of intensity on the beam stop borders. The corrected diffraction pattern from Fig. 4 (a) is shown on Fig. **??**. Reconstruction of the ptychography data

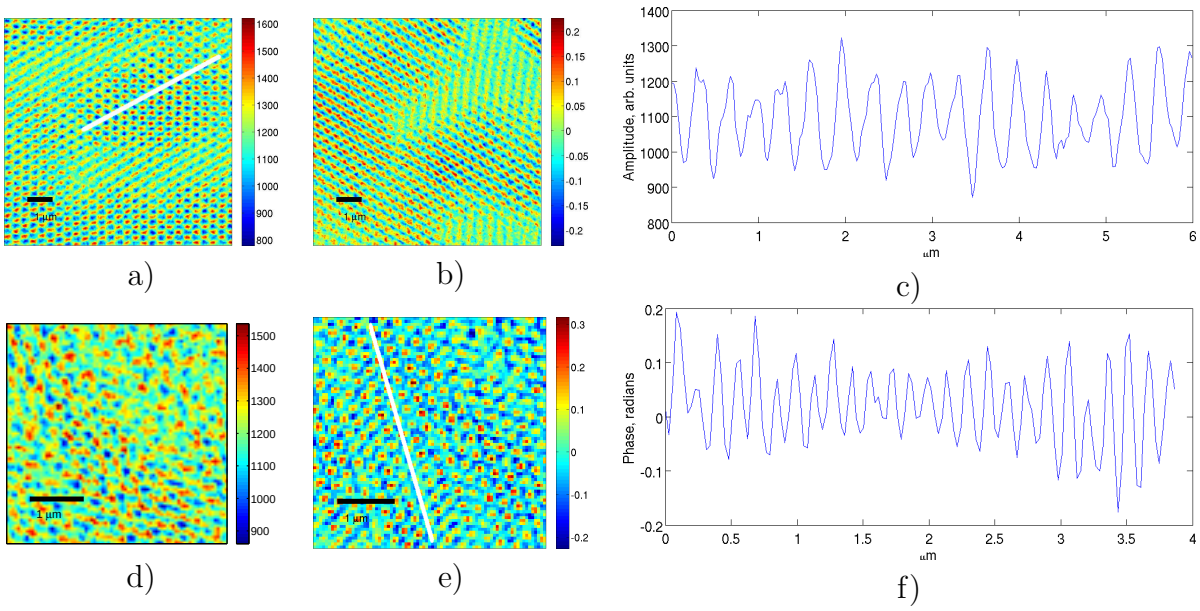

Figure 5: Results of the reconstruction. Top row: 492 nm spheres colloidal crystal sample. Bottom row: 180 nm spheres colloidal crystal sample. (a), (d) object function absolute value; (b), (e) object function phase; (c), (f) line scans along the white lines.

has been carried out using the ePIE algorithm. The algorithm started with a Gaussian probe a uniform object function. The β_1 and β_2 parameters were set to 0.003 and 1, respectively. When reconstructing with higher β_1 values, the probe function starts to incorparate sample features, so that its Fourier transform has Bragg peaks.
The aquired images have been centered, cropped and binned, resulting in 220 μm effective pixel size and 128×128 image resolution. Centering was performed assuming point symmetry of the diffraction pattern. Due to a large number of bad pixels in the upper left quadrant of the detector, the intensity in this quadrant was replaced by an inversion of the diffraction patterns about the diffraction pattern center. Remaining bad pixels and blind zone were filled with interpolated values. As an initial guess for the object function, a uniform distribution has been taken. The initial probe was a Gaussian corresponding to the FWHM values from the beam intensity profiles. The diffraction patterns have been applied in random order.
Results of the reconstruction are shown on Fig. 5. Hexagonal lattices are visible on both reconstructions. The reconstructed lattice parameter for the 492 nm spheres sample is 310 nm, for the 180 nm spheres it is 145 nm. Resolution of the reconstructed image is 28 nm.

4 Conclusions

Reconstruction of periodic samples has been shown to be possible with ptychography. Probe function reconstruction via the ePIE algorithm is limited by the low diversity

of diffraction patterns. The colloidal crystal hexagonal structure has been successfully reconstructed.

References

[1] H. Faulkner and J. Rodenburg. Movable aperture lensless transmission microscopy: A novel phase retrieval algorithm. *Physical Review Letters*, 93(2), Jul 2004.

[2] J. R. Fienup. Reconstruction of an object from the modulus of its fourier transform. *Optics Letters*, 3(1):27, Jul 1978.

[3] J. R. Fienup. Phase retrieval algorithms: a comparison. *Applied Optics*, 21(15):2758, Aug 1982.

[4] R. W. Gerchberg and W. O. Saxton. A practical algorithm for the determination of the phase from image and diffraction plane pictures. *Optik*, 35:237, 1972.

[5] Jacob P. Hoogenboom, Didi Derks, Peter Vergeer, and Alfons van Blaaderen. Stacking faults in colloidal crystals grown by sedimentation. *The Journal of Chemical Physics*, 117(24):11320, 2002.

[6] W. Hoppe. Beugung im inhomogenen primärstrahlwellenfeld. i. prinzip einer phasenmessung von elektronenbeungungsinterferenzen. *Acta Crystallographica Section A*, 25(4):495–501, Jul 1969.

[7] Andrew M. Maiden and John M. Rodenburg. An improved ptychographical phase retrieval algorithm for diffractive imaging. *Ultramicroscopy*, 109(10):1256–1262, Sep 2009.

[8] Janne-Mieke Meijer, Fabian Hagemans, Laura Rossi, Dmytro V. Byelov, Sonja I.R. Castillo, Anatoly Snigirev, Irina Snigireva, Albert P. Philipse, and Andrei V. Petukhov. Self-assembly of colloidal cubes via vertical deposition. *Langmuir*, 28(20):7631–7638, May 2012.

[9] J. M. Rodenburg and R. H. T. Bates. The theory of super-resolution electron microscopy via wigner-distribution deconvolution. *Philosophical Transactions of the Royal Society A: Mathematical, Physical and Engineering Sciences*, 339(1655):521–553, Jun 1992.